Acta Cryst. (1983). A**39**, 524–530

Correlative Microdomain Model for Short-Range-Ordered Alloy Structures. III. Analysis for Diffuse Scattering from Quenched CuAu Alloy

BY S. HASHIMOTO

The Research Institute for Iron, Steel and Other Metals, Tohoku University, Sendai, Japan

(*Received* 2 *September* 1982; *accepted* 7 *January* 1983)

Abstract

Short-range-order diffuse X-ray scattering from a quenched CuAu alloy is analyzed on the basis of the correlative microdomain model [Hashimoto (1974). *Acta Cryst.* A**30**, 792–798; Hashimoto (1981). *Acta Cryst.* A**37**, 511–516]. The average shape of the domains, which have an ordered lattice of the $L1_0$ type, is a spheroid with dimensions of $3{\cdot}1a$ (a = lattice parameter) in the Cu:Au [001] layering direction and $3{\cdot}6a$ in the direction normal to it. The volume fraction of the domains is 0·43 of the crystal volume. Noticeable antiphase relations are found between the domains, which have the same [001] layering and lie on the same (001) plane, with interdomain distance of 30 Å in the ⟨110⟩ directions.

1. Introduction

With the theoretical framework of parts I and II [the correlative microdomain model (CMDM)] (Hashimoto, 1974, 1981*b*) in hand we are now in a position to examine observed diffuse X-ray intensity data on short-range order (SRO) in alloys. Analyses by CMDM have been reported on the disordered Cu–48 at.% Pt (Hashimoto & Iwasaki, 1979) and Cu–29·8 at.% Pd (Oshima & Harada, 1981) alloys. The intensity data from the former alloy were obtained by a photographic method which allows a relatively high-resolution measurement of the intensity distribution to be made. Diffuse maxima appeared at the superlattice reflection points for the $L1_1$-type ordered lattice, but they did not have any fine structure suggesting the presence of the interdomain correlation; the average size and density of the domains were estimated. CMDM analysis was also successfully carried out (Oshima & Harada, 1981) on the X-ray SRO data of Cu–29·8 at.% Pd alloy, which revealed the so-called fourfold splitting on the diffuse maxima (Oshima, Watanabe & Harada, 1976), and the interdomain correlations in antiphase relationship were determined by using a trial-and-error method.

In the present work, we try to analyze diffuse scattering from the 1:1 alloy in the disordered Cu–Au system, in which the fourfold splitting was first noticed on the diffuse maxima located at the superlattice reflection points for the $L1_0$ or $L1_2$ ordered lattice. The splitting was mainly observed by electron diffraction (Hashimoto & Ogawa, 1970) and by X-ray diffraction with the use of a photographic method (Moss, 1965; Yamagishi, Hashimoto & Iwasaki, 1982), because its separation is very narrow. A quantitative measurement on the CuAu alloy by X-ray diffractometry was made by Metcalfe & Leake (1975), but the data did not reveal the fourfold splitting, as far as the intensity contour maps were inspected. The absence of splitting was probably through lack of resolution of the diffractometry adopted.*

We make here a high-resolution measurement of the diffuse intensity distribution from the quenched CuAu alloy by the use of a high-intensity X-ray source and fine slits placed in the beam path on a diffractometer. Applying CMDM to the data obtained, we determine the statistical nature of the microdomains in the model, that is, the average size, the number density of the domains and the spatial interdomain correlations, on the assumption that the internal structure of the domain forms an $L1_0$-type ordered lattice.

Symbols defined in I and II and used in the present paper are listed in Table 1.

2. Method of correction for the atomic-displacement effect

A method to separate the diffuse scattering into components was established by Borie & Sparks (1971) with the assumption that the terms beyond quadratic in $(2\pi\mathbf{q}.\boldsymbol{\Delta})$ may be neglected in the series expansion of $\exp(2\pi i\mathbf{q}.\boldsymbol{\Delta})$, $\boldsymbol{\Delta}$ being a deviation of the interatomic vector from the average. In their method, the volume in reciprocal space to be surveyed in the intensity

* Diffuse scattering from Au–24·4 at.% Cu alloy was observed in a counter method by Harada & Oshima (1978, private communication). They found a fine modulation on its maxima, but no analysis was performed for the data.

0108-7673/83/040524-07$01.50

Table 1. *Glossary*

a	Lattice parameter of the f.c.c. lattice
$\mathbf{R}_{lmn}$	Interatomic vector in the averaged lattice; $\mathbf{R}_{lmn} = l(\mathbf{a}_1/2) + m(\mathbf{a}_2/2) + n(\mathbf{a}_3/2)$, $\lvert\mathbf{a}_j\rvert = a$
$\mathbf{X}$	Vector in real lattice
$\mathbf{q}$	Scattering vector or wave vector in reciprocal space
$\mathbf{q}_l$ or $\mathbf{q}_{\mathbf{G}_l}$	Deviation of the wave vector from $\mathbf{G}_l$; $\mathbf{q}_l \equiv \mathbf{q} - \mathbf{G}_l$
v_o	Crystal volume per atom
n	Total number of atoms in alloy
n_r	Number of atoms composing the random matrix
$\langle n\rangle_t$	Average number of atoms composing a domain of the tth type
N_d	Total number of microdomains
N_t^r	Number of domains of the tth group of order
σ^2	Broadness of the domain-size distribution around the average $\langle n\rangle_t$ defined in the case that the domains have a perfectly ordered lattice within them
$S_t(\mathbf{R}_{lmn})$	Ordering function of the domain of the tth type, which represents the size and shape, by (II-32); $S_t(0) = 1$
$P_{tt'}(\mathbf{X})$	Number density of the domain belonging to the t'th type of order at $\mathbf{X}$, when a domain of the tth type is placed at the origin
$D_0(\mathbf{X})$	Number density for the domain (irrespective of kind) at $\mathbf{X}$ from a domain of the tth type, defined as $D_0(\mathbf{X}) \equiv \sum_{t'} P_{tt'}(\mathbf{X})$
$D(\mathbf{q}_l)$	Reduced intensity around $\mathbf{G}_l$ due to the interdomain correlations; $D(\mathbf{q}_l) \equiv \alpha^l(\mathbf{q}_l)/\alpha^o(\mathbf{q}_l)$
$D_{\mathbf{G}_l}(\mathbf{X})$	Fourier integral of $D(\mathbf{q}_l)$ with respect to $\mathbf{G}_l$; $D_{\mathbf{G}_l}(\mathbf{X}) = P_{tt}(\mathbf{X}) - P_{t,t+3}(\mathbf{X})$ in the $L1_0$ case
α^r	Intensity scattered from the random matrix; $\alpha^r \simeq n_r/n$
$\alpha^m(\mathbf{q}_l)$	Intensity scattered from the microdomains; $\alpha^m(\mathbf{q}_l) \equiv \alpha^o(\mathbf{q}_l) + \alpha^l(\mathbf{q}_l)$
$\alpha^o(\mathbf{q}_l)$	Intensity scattered from the single domains
$\alpha^l(\mathbf{q}_l)$	Intensity modulation due to the interdomain correlation
$\alpha^m_{\mathbf{G}_l}(\mathbf{R}_{lmn})$	Fourier integral of $\alpha^m(\mathbf{q}_l)$ around $\mathbf{G}_l$; $\alpha^m_{\mathbf{G}_l}(\mathbf{R}_{lmn}) \equiv \alpha^o_{\mathbf{G}_l}(\mathbf{R}_{lmn}) + \alpha^l_{\mathbf{G}_l}(\mathbf{R}_{lmn})$
$\alpha^o_{\mathbf{G}_l}(\mathbf{R}_{lmn})$	Fourier integral of $\alpha^l(\mathbf{q}_l)$
$\alpha^l_{\mathbf{G}_l}(\mathbf{R}_{lmn})$	Fourier integral of $\alpha^o(\mathbf{q}_l)$

measurement can be effectively reduced to a very small one by a symmetry of the crystal structure. If the symmetry is lower, a more extensive zone must be surveyed and the measurement and analysis become much more complicated. In our preliminary experiment, there was a small but appreciable difference in intensity between the diffuse maxima at the 110, 101 and 011 superlattice reflection points from a sample crystal with its face parallel to the (111) plane. These maxima should be symmetrical about the [111] axis, if the cubic symmetry is to be retained, but the intensity ratio of the three diffuse maxima was 1·00:1·05:1·21. This suggests the existence of anisotropy in the crystal, which is thought to originate from a coupling of the atomic ordering and dislocations or subgrain boundaries with preferential orientation generated during crystal growth. Therefore, the Borie–Sparks method could not be used for the present alloy, and instead the following method was adopted. We measure the intensity distribution around the 110 reflection point, since it is positioned at a lower scattering angle and is considered to be little affected by the atomic-displacement effect. The intensity modulation due to the atomic displacements is written as, in Laue units,

$$I_{\mathrm{ad}}(\mathbf{q}) = -\sum_{lmn} (h_1 \gamma^x_{lmn} + h_2 \gamma^y_{lmn} + h_3 \gamma^z_{lmn}) \times \sin \pi(h_1 l + h_2 m + h_3 n), \quad (1)$$

where γ^x_{lmn} *etc.* are the first-order atomic-displacement parameters defined by Sparks & Borie (1965). The average of the intensities at two points, $1 - \Delta h_1$, $1 - \Delta h_2$, $0 - \Delta h_3$ and $1 + \Delta h_1$, $1 + \Delta h_2$, $0 + \Delta h_3$, around the 110 point can be calculated as

$$\{\Delta h_1 \gamma^x_{lmn} + \Delta h_2 \gamma^y_{lmn} + \Delta h_3 \gamma^z_{lmn}\} \times \sin \pi(\Delta h_1 l + \Delta h_2 m + \Delta h_3 n).$$

In the case that the diffuse scattering is highly concentrated at the 110 point, this atomic-displacement term has negligible magnitude. On the other hand, the pure SRO intensity part is centrosymmetric about the 110 point.

3. Experimental procedures

The materials used in the preparation of the alloy were copper and gold both of 99·99% purity. Using the Bridgman technique, a CuAu single-crystal rod of 13 mm diameter was grown in a graphite crucible kept in a vacuum and then rapidly cooled. The ingot was encapsulated in an evacuated quartz tube, homogenized at 1073 K for a week and then quenched into water. Composition of the alloy thus prepared was determined by measuring the lattice parameter, a, with reference to the established relation between a and the composition (Jehanno, 1965). A powder specimen filed from the bulk crystal gave a = 3·893 Å, which indicated a composition of Cu–53 at.% Au. A sample slice was cut from the bulk single crystal with two faces parallel to the (210) plane, encapsulated in a Pyrex tube, annealed at 773 K for a month and at 738 K for a week and then quenched into ice–water. A good metallographic surface was prepared by alternately hand polishing and electropolishing in a solution of phosphoric acid and chromic acid. A final Laue pattern indicated a mosaic spread of less than $\frac{1}{2}°$.

Diffuse-scattering measurement was made with an X-ray diffraction system consisting of a Rigaku RU-200 rotating-Cu-anode generator, a sodium-iodide scintillation counter with pulse-height analyzer, a modified Rigaku SG-7 goniometer (with θ and 2θ axes) and a single-crystal orienter (with χ and φ axes), designed for this work (Hashimoto, Yamagishi, Iwasaki, Wagatsuma, Yoshizawa & Yamada, 1980). The incident beam was monochromated with a flat pyrolitic graphite and its cross section at the sample position was 0·8 mm in diameter. The horizontal divergence of the incident beam due to the mosaic spread of the monochromator was measured to be less than 0·3° and the vertical divergence was estimated to be 0·2° from the X-ray optical geometry. Divergences of the scattered beam were 0·4° (horizontal) and 0·2° (vertical). These divergences were much smaller than those reported, for example 1·3° (h) and 2·2° (v) by Metcalfe & Leake (1975). Total divergence can be

represented by the volume of resolution with approximate dimensions of $(0{\cdot}005)^3$ Å^{-3} at $2\theta = 90°$. Each side of the volume corresponds to $\frac{1}{100}$ the distance from the origin to the 200 fundamental reflection point. With two rotations provided by the goniometer, the sample face could be maintained symmetrical with respect to the incident and diffracted beams, so as to have an absorption factor independent of 2θ. The nickel–cobalt balanced filters were used to eliminate the half-wavelength component from the monochromator. Diffuse-intensity measurements were made through a volume shown in Fig 1. This volume is twice the minimum repeating unit of the pure SRO diffuse intensity from a f.c.c. alloy. Measurements were made at the points spaced at intervals of $\delta h_1 = \delta h_2 = \delta h_3 = \frac{1}{40}$ in the vicinity of the peak position of the diffuse maximum. The intervals were nearly equal to the dimensions of the volume of resolution and were about $\frac{1}{3}$ the separation of the splitting on the diffuse maximum previously reported (Hashimoto & Ogawa, 1970; Yamagishi, Hashimoto & Iwasaki, 1982). The region with a monotonically varying intensity was surveyed at wider intervals. No measurement was made at the point with $h_3 > 0{\cdot}9$ because there was uncertain temperature diffuse scattering and Huang diffuse scattering as a tail of the strong 111 fundamental reflection. The measured intensities were converted to absolute units (electron units per atom) by comparing with the scattering intensity at $2\theta = 100°$ from polystyrene. Atomic scattering factors and their dispersion corrections given in *International Tables for X-ray Crystallography* (1974) were used. The intensity for each sampling point was corrected for air scattering and Compton scattering by a method described in a previous paper (Hashimoto, 1981*a*).

Subtraction of the atomic-displacement modulations was carried out in the way described in § 2. The averaging of intensity was, in practice, made between the two points, one in the upper half and the other in the lower half of the volume shown in Fig. 1 cut off by a plane $h_1 + h_2 = 2$, taking into consideration the symmetry of the intensity distribution around the 110 point.

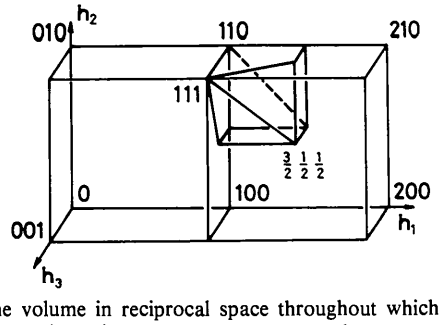

Fig. 1. The volume in reciprocal space throughout which diffuse intensity measurements were made.

4. Experimental results

Values of the SRO diffuse intensity were interpolated onto a cubic net of points spaced at intervals of $\delta h_1 = \delta h_2 = \delta h_3 = \frac{1}{40}$ over the whole volume in Fig. 1. Figs. 2(*a*) and (*b*) show the intensity contours around the 110 point on the (110) and (001) sections in reciprocal space, respectively. The intensity data thus collected reveal a characteristic shape. The splitting of the diffuse maximum can be more clearly seen in the intensity profiles of $\alpha^m(q)$ across the 110 point, as shown in

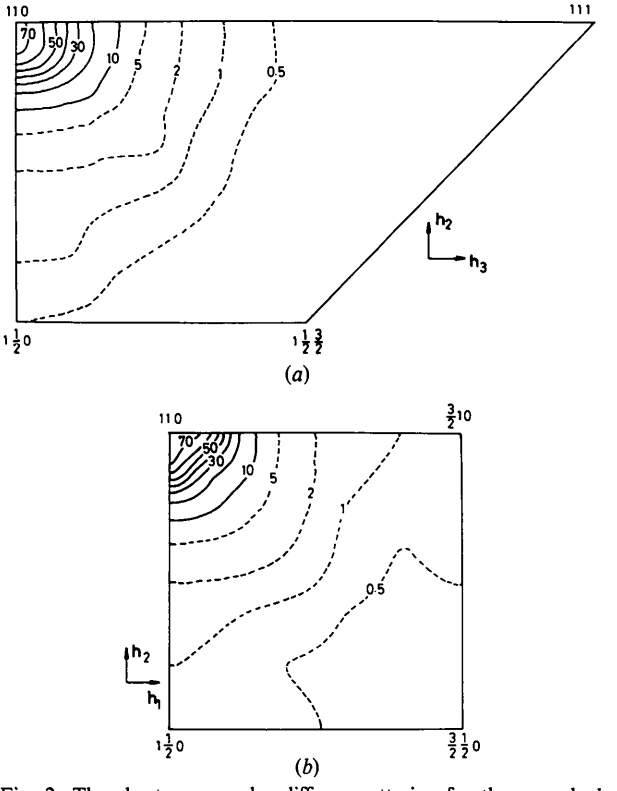

Fig. 2. The short-range-order diffuse scattering for the quenched Cu–53 at.% Au (*a*) on the (100) section, (*b*) on the (001) section.

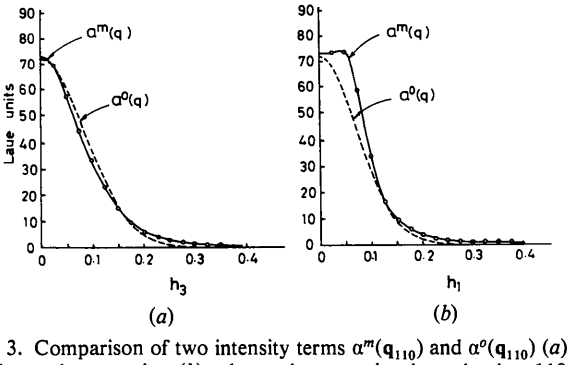

Fig. 3. Comparison of two intensity terms $\alpha^m(\mathbf{q}_{110})$ and $\alpha^o(\mathbf{q}_{110})$ (*a*) along the *z* axis, (*b*) along the *x* axis through the 110 reciprocal-lattice point. The solid line gives $\alpha^m(\mathbf{q}_{110})$ and the dashed line $\alpha^o(\mathbf{q}_{110})$.

Fig. 3. In Fig. 2 the diffuse maximum decreases in magnitude as fast as $\exp(-17a|\mathbf{q}_{110}|)$ at its tail and the measured intensity midway between this maximum and the neighboring diffuse maxima can be regarded as the level of uniform background. A tail of considerably strong diffuse intensity (TDS, Huang and higher-order static displacement effects) was found even in the measured volume of $h_3 \leq 0{\cdot}9$ as well, and it had a peculiar form of distribution, perhaps due to the Huang scattering. This intensity was removed, assuming that the SRO intensity was uniform under the strong diffuse intensity.

In Fourier integration of the intensity around the 110 point over the volume in Fig. 1, the effect of a truncation by the surfaces of the volume may be caused by a uniform background α^r, since the intensity coming from the microdomains, $\alpha^m(\mathbf{q}_{110})$, damps rapidly with increasing $|\mathbf{q}_{110}|$. Hence, the integrations required for the present CMDM analysis were carried out after subtracting the uniform background to such an extent that the effect of the truncation was small.

Following the procedures described in II, we started the analysis by Fourier integrating the observed intensity, $\alpha^m(\mathbf{q}_{110})$ and separating it into the components $\alpha^o_{110}(\mathbf{R}_{lmn})$ and $\alpha^l_{110}(\mathbf{R}_{lmn})$. The relation between these components is illustrated in Fig. 4 in II, where, for the sake of brevity, only one diffuse maximum is assumed to exist in the Brillouin zone. $\alpha^o_{110}(\mathbf{R}_{lmn})$ is a smooth function representing the contribution from the single domains and has a non-zero value within an intermediate distance of $\mathbf{R}_{lmn}$. $\alpha^l_{110}(\mathbf{R}_{lmn})$, an oscillating function arising from interdomain correlations, extends over the wider range of $\mathbf{R}_{lmn}$. As a function describing $\alpha^o_{110}(\mathbf{R}_{lmn})$, we chose a product of Gaussian functions as

$$\alpha^o_{110}(\mathbf{R}_{lmn}) = a \exp[-b(l^2 + m^2) + cn^2], \qquad (2)$$

and the constants a, b and c were determined by least-squares fitting of this function to $\alpha^m_{110}(\mathbf{R}_{lmn})$. In this fitting procedure, the values of $\alpha^m_{110}(\mathbf{R}_{lmn})$ greater than $\alpha^o_{110}(\mathbf{R}_{000})/10$ were used and a, b and c were determined to be $0{\cdot}13_8$, $0{\cdot}026_8$ and $0{\cdot}037_2$, respectively.

The fraction of the atoms constructing the random matrix in the whole crystal is given by

$$\begin{aligned} n_r/n &= 1 - [\alpha^o_{110}(\mathbf{R}_{000}) + \alpha^o_{101}(\mathbf{R}_{000}) + \alpha^o_{011}(\mathbf{R}_{000})] \\ &= 1 - \alpha^o_{110}(\mathbf{R}_{000})(1 + 1{\cdot}05 + 1{\cdot}21) = 0{\cdot}57. \end{aligned} \qquad (3)$$

As the abundance ratio of the domains belonging to the different types of order used in this equation, the values obtained from the crystal cut with (111) face were adopted. In Table 2, $\alpha^m_{110}(\mathbf{R}_{lmn})$, the Fourier integral of the observed total intensity, and $\alpha^o_{110}(\mathbf{R}_{lmn})$ are compared. The fitting is seen to be good in the whole range listed in the table, but a relatively large discrepancy still remains in the range of small $\mathbf{R}_{lmn}$. The difference could be due to the presence of a weak nearest-neighbor-pair correlation in the random matrix. Thus, α^r should be regarded as a slowly varying function in the present case rather than a uniform function of value n_r/n. Fig. 3 shows profiles of $\alpha^m(\mathbf{q}_{110})$ and $\alpha^o(\mathbf{q}_{110})$ along the [100] and [001] directions through the 110 point in reciprocal space. The difference between the solid line for $\alpha^m(\mathbf{q}_{110})$ and the dotted line for $\alpha^o(\mathbf{q}_{110})$ gives the interdomain interference term $\alpha^i(\mathbf{q}_{110})$. It can be seen in the figures that $\alpha^i(\mathbf{q}_{110})$ has some oscillating form. We now calculate the function $D(\mathbf{q}_{110})$* and Fourier integrate it to obtain the interdomain correlation.

Table 2. *Comparison of* $\alpha^m_{111}(\mathbf{R}_{lmn})$ *and* $\alpha^o_{110}(\mathbf{R}_{lmn})$

$l\,m\,n$	$\alpha^m_{110}(\mathbf{R})$	$\alpha^o_{110}(\mathbf{R})$
0 2 0	0·168	0·120
2 2 0	0·122	0·108
0 4 0	0·097	0·087
2 4 0	0·078	0·078
4 4 0	0·051	0·057
0 6 0	0·041	0·051
2 6 0	0·042	0·046
4 6 0	0·030	0·033
0 8 0	0·025	0·024
0 0 2	0·163	0·116
0 2 2	0·124	0·104
2 2 2	0·103	0·093
0 4 2	0·073	0·075
2 4 2	0·064	0·067
4 4 2	0·048	0·049
0 6 2	0·041	0·044
2 6 2	0·037	0·039
4 6 2	0·029	0·028
0 0 4	0·077	0·074
0 2 4	0·063	0·066
2 2 4	0·056	0·059
0 4 4	0·045	0·048
2 4 4	0·041	0·043
4 4 4	0·033	0·031
0 6 4	0·029	0·028
2 6 4	0·026	0·025
0 0 6	0·032	0·035
0 2 6	0·028	0·031
2 2 6	0·027	0·028
0 4 6	0·024	0·023
2 4 6	0·022	0·021

$$D_{110}(\mathbf{X}) \equiv P_{11}(\mathbf{X}) - P_{14}(\mathbf{X}). \qquad (4)$$

This function is expressed as a difference of the two kinds of correlations, one between the domains both belonging to the first type of order and the other between the domains belonging to the first and fourth types defined in Fig. 1 of II, which are in the same group with their unique axes along the z axis of the cubic lattice. That is, $D_{110}(\mathbf{X})$ is a function showing whether the in-phase or out-of-phase relation is

* Both $\alpha^i(\mathbf{q}_i)$ and $\alpha^0(\mathbf{q}_i)$ tend to zero as $|\mathbf{q}_i|$ increases, and $D(\mathbf{q}_i)$ becomes indeterminate at large $|\mathbf{q}_i|$. Therefore, we used $D(\mathbf{q}_i) = \alpha^i(\mathbf{q}_i)/\varepsilon$ for $|\mathbf{q}_i| > 0{\cdot}17/a$, where $\alpha^0(\mathbf{q}_i) \leq \varepsilon$. ε was taken to be $\alpha^0(\mathbf{q}_i = 0)/10$. The interdomain interference term $\alpha^i(\mathbf{q}_i)$ which arises from the relatively long-range correlation may have a significant contribution to the central range of the diffuse maximum and no fatal error is involved in this approximation.

enhanced for the domain pairs at the interdomain distance of **X**. Fig. 4 shows contours of $v_o D_{110}(\mathbf{X})$ on the (001), (110) and (010) sections in real space, which are in units of the number of domains per atom. There exists a negative peak at $\mathbf{X} = 11(a/2)(1,1,0)$ ($\simeq 30$ Å) and two small positive peaks at $12(a/2)(1,0,0)$ ($\simeq 23$ Å) and $6(a/2)(1,1,1)$ ($\simeq 20$ Å). The negative peak, which explains an enhancement of the antiphase relation between the domains, plays an important role in generating the fourfold splitting observed on the diffuse maximum.

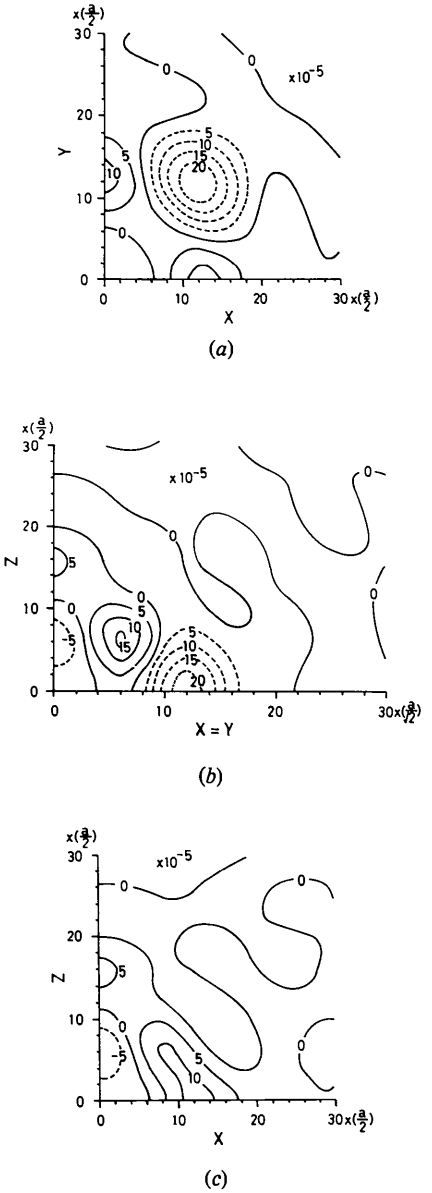

Fig. 4. Contours of the interdomain correlation function $v_o D_{110}(\mathbf{X})$ for the domains with their unique axes along the z axis. (*a*) (001), (*b*) (110) and (*c*) (010) sections.

From the function $\alpha^o(\mathbf{q}_{110})$ obtained, we could derive the following three quantities;

$$A \equiv v_o \int \alpha^o(\mathbf{q}_{110})\, d\mathbf{q}_{110} = 0{\cdot}13, \tag{5a}$$

$$B \equiv \alpha^o(\mathbf{q}_{110} = 0) = 70, \tag{5b}$$

$$C \equiv v_o \int \{\alpha^o(\mathbf{q}_{110})\}^{1/2} d\mathbf{q}_{110} = 0{\cdot}044. \tag{5c}$$

If a step function as defined by (I-6) is assumed as the shape of the domain, we can calculate N_1'/n, $\langle n\rangle_1$ and σ^2 by $AC/B^{1/2}$, $B^{1/2}/C$ and $B^{3/2}/(AC) - B/C^2$, respectively, with the result $N_1'/n = 0{\cdot}00068$, $\langle n\rangle_1 = 190$ and $\sigma^2 = 65\,000$. The value of σ^2 is much greater than $\langle n\rangle_1^2 = 35\,000$, although this was expected when the function given in (2) was chosen as the smooth function $\alpha^o_{110}(\mathbf{R}_{lmn})$. Hence, the shape of domains in the present alloy is characterized rather by an 'ordering function' $S_1(\mathbf{R}_{lmn})$. In this case, the equations related to the parameters must be redefined as $N_1'/n = C^2$ and $\langle n\rangle_1 = A/C^2$, following II.

The parameters characterizing the domain structure are listed in Table 3.

5. Discussion

The difference between the interdomain correlation functions $P_{1t}(\mathbf{X})$'s was obtained from (4), but $P_{1t}(\mathbf{X})$ itself could not be calculated directly from the diffuse intensity. We suggested for the case of the $L1_2$-type internal structure in II that if a quantity $D_0(\mathbf{X}) \equiv \sum_t P_{1t}(\mathbf{X})$ is known, each $P_{1t}(\mathbf{X})$ can be calculated as (II-34).

In the case of the $L1_0$ type, if the fractions of the domains belonging to the three groups of order are the same and if $D_0(\mathbf{X})$ is known, $P_{1t}(\mathbf{X})$'s can be obtained through the relation

$$P_{11}(\mathbf{X}) = D_0(\mathbf{X})/6 + D_{110}(\mathbf{X})/2, \tag{6a}$$

$$P_{14}(\mathbf{X}) = D_0(\mathbf{X})/6 - D_{110}(\mathbf{X})/2. \tag{6b}$$

The common term $D_0(\mathbf{X})/6$ is cancelled out in (II-1*e*) and hence the SRO diffuse scattering is not affected by $D_0(\mathbf{X})$.

We try to deduce $D_0(\mathbf{X})$ from an analogy with a liquid structure. For simplicity, let the shape of the domains be a hard sphere with diameter d given by

$$\frac{4}{3}\pi\left(\frac{d}{2}\right)^3 = \frac{4}{3}\pi\left(\frac{d_c}{2}\right)\left(\frac{d_b}{2}\right)^2, \tag{7}$$

Table 3. *Parameters of the domain structure*

Ordering function: $S_1(\mathbf{R}_{lmn})$	$\exp[-0{\cdot}053_5(l^2+m^2) - 0{\cdot}074_4 n^2]$
Fraction of the disordered atoms: n_r/n	0·57
The number of ordered atoms in a domain: $\langle n\rangle_1$	66 atoms
Crystal volume per domain: $nv_o/\sum_t N_t'$	$155v_o$
Dimensions of a domain	$d_b = 3{\cdot}6a$, $d_c = 3{\cdot}1a$
Characteristic interdomain correlation: $v_o D_{110}(\mathbf{X})$	Negative peak at $11(a/2)$ (1,1,0)

where d_c and d_b are dimensions of a spheroidal contour at the half value of the ordering function along the principal axis and its normal, respectively. In the present case, d_c and d_b are $3{\cdot}1a$ and $3{\cdot}6a$, respectively, and hence $d = 3{\cdot}4a$.

According to Ashcroft & Lekner (1966), the direct correlation function in reciprocal space is given on the basis of the Percus–Yevick approximation (Percus & Yevick, 1958; Percus, 1962) by

$$C(q) = -4\pi d^3 \int_0^1 \mathrm{d}s\, s^2 \frac{\sin(sq)}{sq} (\alpha + \beta s + \gamma s^3). \quad (8)$$

The parameters α, β and γ are functions of a packing-density parameter $\eta = (\pi/6)\rho_o d^3$ (ρ_o: number density of the spheres),

$$\alpha = (1 + 2\eta)^2/(1 - \eta)^4,$$
$$\beta = -6\eta(1 + \eta/2)^2/(1 - \eta)^4,$$
$$\gamma = (\tfrac{1}{2})\,\eta(1 + 2\eta)^2/(1 - \eta)^4.$$

The pair correlation function $g(r)$ defined in a liquid structure can be calculated by

$$g(r) - 1 = \frac{1}{2\pi^2\rho_0} \int_0^\infty [S(q) - 1] \frac{\sin(qr)}{qr} q^2\,\mathrm{d}q, \quad (9)$$

where $S(q)$ is given from the Ornstein–Zernike equation as

$$S(q) = 1/[1 - \rho_o C(q)]. \quad (10)$$

In the present case, $g(r)$ corresponds to $D_0(X)/\rho_o$. Parameters required in the calculation of $D_0(X)$ are ρ_o and d, and ρ_o is given as

$$\rho_o = \frac{N_d}{V} = \sum_{t=1}^{3} N_t'/(nv_o) = 0{\cdot}00198(1 + 1{\cdot}05 + 1{\cdot}21)/v_o$$
$$= 0{\cdot}00645/v_o, \ (V\text{: crystal volume}). \quad (11)$$

Then we have

$$v_o D_0(X) = 0{\cdot}00645 g(X). \quad (12)$$

This is a radial (random) distribution function giving the number of the spherical domains within a volume v_o ($= a^3/4$ for f.c.c.). Fig. 5 shows the function $v_o D_0(X)$ calculated. It has a sharp peak at the distance equal to the diameter of the domain, rapidly decreases in an oscillating manner and tends to the average density of the domains. Comparison of the first peak in Fig. 5 and the contour maps in Fig. 4 shows that there is no preferential pairing between the order types of domains, in-phase or out-of-phase, at the distance $X = 7(a/2)$. The positive and negative peaks in the contour maps in Fig. 4 are found to be located approximately at the positions of the second and third peaks in the radial distribution of the domains given in Fig. 5. This suggests that the antiphase correlations exist between the domains at relatively long distances apart. It is to be noted that the antiphase correlation is weak, the corresponding number density being lower than $\frac{1}{30}$ the average number density of the domains.

The domain structure analyzed here may be understood by an illustration (two-dimensional drawing) as shown in Fig. 6. Circles indicate the domains with their unique axes along the z axis and ellipses those with their unique axes along the x and y axes. The phase relation is represented by the signs (+ and −). The domain pairs associated with the negative peaks in $v_o D_{110}(\mathbf{X})$ are indicated by the arrows. The shaded region is the random matrix, where, in the present case, a low degree of nearest-neighbor ordering exists.

Interdomain interaction corresponding to the fine structures on the diffuse maxima has been considered to be caused by the conduction-electron energy, *i.e.* the Fermi-surface nesting effect. Moss (1969) suggested that the factors affecting the phenomenon are (1) the flatness of the Fermi surface in the direction of interest and (2) the diffuseness of the Fermi surface at the

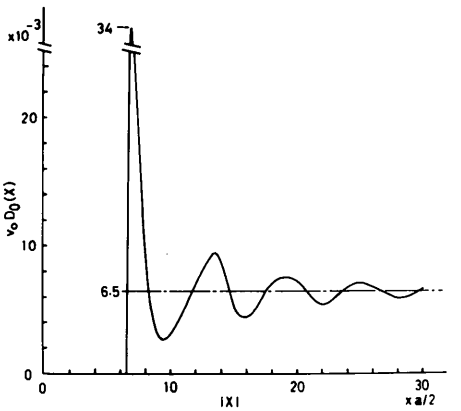

Fig. 5. Radial distribution function of $v_o D_0(X)$.

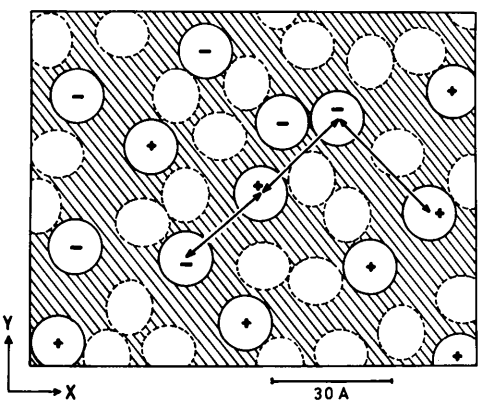

Fig. 6. Schematic illustration of the microdomain structure in the Cu–53 at.% Au alloy. Circles indicate the domains with their unique axes along the z axis, and ellipses the domains with their axes along the x and y axes. The +/− sign represents the phase relation. Arrows indicate the domain pairs corresponding to the negative peak in $v_o D_{110}(\mathbf{X})$.

temperature in question. The latter factor may be divided into (*a*) the lattice vibration and (*b*) the disordering of the constituent atoms arising from the configurational entropy term. Here, let the latter effect be considered. The Fermi surface is sharp if the conduction electrons propagate in a periodic field of the crystal without being scattered. In the path of propagation, the higher the degree of atomic ordering is, the more serious the singularity in the conduction-electron energy is. Therefore, the considerably long-range interdomain correlation is considered to be stronger in the portions where the microdomains accidentally gather together. The $2\mathbf{k}_F$ loci of the Fermi surface imaged in the diffraction patterns may be effectively enhanced by the presence of the highly ordered regions or the microdomains and the contact between them. On the other hand, local ordering within the domains is caused mainly by the atomic-size effect (or core repulsive interaction) rather than the conduction-electron-energy effect. It is only when strong short-range interatomic interactions such as the atomic-size effect exist that the Fermi-surface effect is generated in the alloy, even though the Fermi surfaces for the constituent metals have flat portions.

Here, we think again about the average size of the domains. If two domains of the same type of order are in contact, one large domain is produced there, instead of the two small domains. We must have a criterion to know whether this locally ordered region is to be interpreted as a contact of two domains or a large single domain. See Fig. 7, where two domains in (*a*) in-phase relation and (*b*) out-of-phase relation are in contact. If the two cases are equally probable in the alloy crystal, the two kinds of domain can be considered to be independently correlated to one another and the average size of the domains is defined as that of each one. In the present analysis, such interpretation on the domain size must be taken. One may find domains in electron-microscopic images or on a section of an alloy structure generated by a computer simulation which are larger than the average size determined by the present analysis.

In real alloy crystals, another kind of interdomain correlation, *e.g.* that through strain fields around the domains, may exist. The diffraction effect from the strains in the vicinity of the domains appears particularly around the fundamental reflections as the Huang scattering and the higher-order atomic-displacement effect. The peculiar form of the strong diffuse scattering intensity observed around the fundamental reflection is thought to be due to the lower symmetry of microlayering in the domains. The strain field can cause interdomain correlations between the different groups of order, but does not remarkably affect the SRO diffuse scattering. We infer that the effect appears around the fundamental reflection points, as the Huang scattering with a peculiar form involves information about the strain fields and the spatial correlation between the different groups. Analysis of this type of diffuse scattering remains as a future problem.

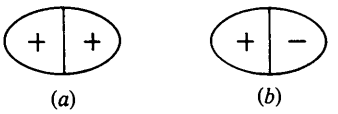

Fig. 7. Contact of two domains. (*a*) (+/+) = in-phase relation and (*b*) (+/−) = out-of-phase relation.

The author wishes to thank Professor H. Iwasaki for valuable comments and revision of the manuscript and Dr M. Misawa for useful comments on the liquid model. The present work has partly been supported by Grant-in-Aid for Developmental Scientific Research from the Ministry of Education, Science and Culture.

References

ASHCROFT, N. W. & LEKNER, J. (1966). *Phys. Rev.* **145**, 83–90.
BORIE, B. S. & SPARKS, C. J. (1971). *Acta Cryst.* A**27**, 198–201.
HASHIMOTO, S. (1974). *Acta Cryst.* A**30**, 792–798.
HASHIMOTO, S. (1981*a*). *Sci. Rep. Res. Inst. Tohoku Univ. Ser. A*, **30**, 44–59.
HASHIMOTO, S. (1981*b*). *Acta Cryst.* A**37**, 511–516.
HASHIMOTO, S. & IWASAKI, H. (1979). *Phys. Status Solidi A*, **51**, 673–682.
HASHIMOTO, S. & OGAWA, S. (1970). *J. Phys. Soc. Jpn*, **29** 710–721.
HASHIMOTO, S., YAMAGISHI, K., IWASAKI, H., WAGATSUMA, H., YOSHIZAWA, K. & YAMADA, T. (1980). *Sci. Rep. Res. Inst. Tohoku Univ. Ser. A*, **29**, 79–101.
International Tables for X-ray Crystallography (1974). Vol. IV. Birmingham: Kynoch Press.
JEHANNO, G. (1965). Thesis. Univ. de Paris.
METCALFE, E. & LEAKE, J. A. (1975). *Acta Metall.* **23**, 1135–1143.
MOSS, S. C. (1965). In *Local Atomic Arrangements Studied by X-ray Diffraction*, edited by J. B. COHEN & J. E. HILLIARD, pp. 95–122. New York: Gordon & Breach.
MOSS, S. C. (1969). *Phys. Rev. Lett.* **22**, 1108–1111.
OSHIMA, K. & HARADA, J. (1981). *Sci. Rep. Res. Inst. Tohoku Univ. Ser. A*, **29**, Suppl. 1, 123–128.
OSHIMA, K., WATANABE, D. & HARADA, J. (1976). *Acta Cryst.* A**32**, 883–892.
PERCUS, J. K. (1962). *Phys. Rev. Lett.* **8**, 462–463.
PERCUS, J. K. & YEVICK, G. J. (1958). *Phys. Rev.* **110**, 1–13.
SPARKS, C. J. & BORIE, B. (1965). In *Local Atomic Arrangements Studied by X-ray Diffraction*, edited by J. B. COHEN & J. E. HILLIARD, pp. 5–46. New York: Gordon & Breach.
YAMAGISHI, K., HASHIMOTO, S. & IWASAKI, H. (1982). *J. Phys. Soc. Jpn*, **51**, 605–611.